

Toward Accurate and Reliable Iris Segmentation Using Uncertainty Learning

Jianze Wei^{1,2}, Huaibo Huang², Muyi Sun², Ran He², Zhenan Sun²

¹ School of Artificial Intelligence, University of Chinese Academy of Sciences, Beijing, China

² CRIPAC & NLPR, Institute of Automation, Chinese Academy of Sciences, Beijing, China
{jianze.wei, huaibo.huang, muyi.sun}@cripac.ia.ac.cn, {rhe, znsun}@nlpr.ia.ac.cn

Abstract

As an upstream task of iris recognition, iris segmentation plays a vital role in multiple subsequent tasks, including localization and matching. A slight bias in iris segmentation often results in obvious performance degradation of the iris recognition system. In the paper, we propose an Iris U-transformer (IrisUsformer) for accurate and reliable iris segmentation. For better accuracy, we elaborately design IrisUsformer by adopting position-sensitive operation and repackaging transformer block to raise the spatial perception ability of the model. For better reliability, IrisUsformer utilizes an auxiliary head to distinguish the high- and low-uncertainty regions of segmentation predictions and then adopts a weighting scheme to guide model optimization. Experimental results on three publicly available databases demonstrate that IrisUsformer achieves better segmentation accuracy using 35% MACs of the SOTA IrisParseNet. More importantly, our method estimates the uncertainty map corresponding to the segmentation prediction for subsequent processing in iris recognition systems.

Introduction

With the increasing demands of biometrics available in the non-contact and masked face scenario, researchers gradually consider achieving personal identification using ocular biometrics, including iris recognition known for its high accuracy. Iris pattern builds its uniqueness through the rich texture details (such as freckles, coronas, crypts, furrows, etc.) (Sun and Tan 2008; He et al. 2008), which establishes a solid cornerstone in the high accuracy of iris recognition. To find the discriminative clue for recognition, iris segmentation is proposed to divide the valid region that contains rich iris texture from the ocular image.

Since iris segmentation is the first primary task that follows the image acquisition, its performance directly or indirectly affects the final recognition accuracy. Specifically, from the partial process perspective of biometric, the segmentation prediction directly drives the localization prediction, i.e., parameters of inner and outer circles of iris boundaries (Wildes 1997). From the perspective of the overall process, the segmentation prediction determines valid regions in feature matching (Zhao and Kumar 2017). In summary,

iris segmentation influences multiple subsequent processes of iris recognition, and slight bias in segmentation would exponentially affect the final recognition performance. Therefore, *it is crucial for iris recognition to obtain iris segmentation results with high accuracy and high reliability.*

Accuracy: To accomplish accurate iris segmentation, some pioneering works are proposed based on extra prior knowledge, such as circular boundary assumption (Daugman 1993; Wildes 1997), total variance (Zhao and Ajay 2015), low-resolution contour (Sutra, Garcia-Salicetti, and Dorizzi 2012). With the development of deep iris segmentation, researchers realize that it is feasible to achieve segmentation by exploring the intrinsic knowledge in the images. MFCNs (Liu et al. 2016) and FCDNN (Bazrafkan, Thavalengal, and Corcoran 2018) provide an end-to-end solution for noisy iris segmentation. IrisParseNet (Wang et al. 2020) proposes a multi-scale attention module and embeds it into the Unet (Ronneberger, Fischer, and Brox 2015) to predict the segmentation mask and outer boundary simultaneously. These works gradually reveal the fact that intrinsic knowledge for iris segmentation is hidden in the local contextual aggregation. Recently, the visual transformer rises rapidly and shows an impressive performance in semantic segmentation task (Liu et al. 2021; Zheng et al. 2020). Different from previous CNN models, transformers employ a self-attention mechanism to explore long-range dependencies in the image and mitigate the limited context modeling problem.

Inspired by the above analysis, we propose a hierarchical encoder-decoder network named IrisUsformer (Iris U-Transformer) for accurate segmentation by exploring local and global contextual aggregation with visual transformer. Considering that iris segmentation is a task sensitive to spatial position, IrisUsformer is elaborately designed for iris segmentation with the following two efforts. First, IrisUsformer utilizes convolutional projection to improve the perception of spatial information. Specifically, conventional visual transformer models rely on only position embedding for the spatial position, and the rest of the transformer pays less mind to the impact of the position on segmentation accuracy. IrisUsformer repackages the transformer block and replaces linear projections with convolutional projections for better spatial perception. The repackaged block can well work with

convolution modules that are sensitive to spatial information. Second, IrisUsformer adopts a U-shaped architecture to build a symmetric structure for the extraction and fusion of hierarchical features. Previous literature demonstrates that a U-shaped architecture network is a powerful model in iris segmentation since it generates hierarchical features with multiple scales. Upon this architecture, IrisUsformer improves the interaction between segmentation prediction and hierarchical features according to the cross-attention mechanism, improving the segmentation accuracy.

Reliability: Reliability is one of the hot issues for deep learning in recent years, while it is less considered in iris segmentation. In our opinion, the reliability in iris segmentation is driven by two aspects, annotation and model uncertainty. The segmentation annotation for the iris region is highly connected with the subjective feelings of annotators. The anatomical characteristics of the eyeball (Jain, Flynn, and Ross 2007) make it hard for annotators to obtain a reliable segmentation annotation, especially the pixels in the iris boundary. Model uncertainty is another inevitable challenge for reliability due to limited data (Zheng and Yang 2021).

To learn reliable segmentation prediction, an uncertainty-wise weighting scheme is proposed to guide the model to pay more attention to the unreliable region with high uncertainty. Specifically, IrisUsformer introduces an auxiliary head to predict additional segmentation and utilizes the discrepancy between segmentation results from the segmentation head and auxiliary head to estimate the uncertainty map. According to the estimated map, IrisUsformer weights the high-uncertainty region with a large value to mitigate uncertainty and the low-uncertainty region with a small value to avoid overtraining. Meanwhile, IrisUsformer adopts an uncertainty regularizer to improve its reliability further.

The main contributions are summarized as follows:

- A hierarchical encoder-encoder network named IrisUsformer is proposed based on the visual transformer for accurate and reliable iris segmentation. IrisUsformer adopts position-sensitive operation and re-packages transformer block to improve spatial perception. The decoder utilizes a cross-attention mechanism to upgrade the interaction between hierarchical features and segmentation predictions.
- We propose an uncertainty-wise weighting scheme by utilizing an auxiliary head to improve the segmentation reliability. The proposed scheme estimates the uncertainty map according to the inconsistency of the segmentation predictions and further reduces the high-uncertainty region via a weighting strategy.
- The superior performance on three challenging iris datasets demonstrates the effectiveness of the proposed IrisUsformer. In addition, an ablation study and visualization experiment are conducted to understand the contributions of each module to performance improvement.

Related work

Iris segmentation

A complete iris recognition consists of four parts, image acquisition, pre-processing, feature extraction, and matching. Iris segmentation is an important step of pre-processing, and it defines the valid iris region for subsequent tasks.

Conventional iris segmentation approaches pursue accurate iris segmentation by using extra prior knowledge or assumption. One of the most famous assumptions is the circular assumption (Daugman 1993; Wildes 1997), i.e., the inner and outer boundaries of the iris region can be regarded as the perimeters of two parameterized circulars. Since circle parameters are also the goal of the iris localization task, it is hard to distinguish iris segmentation and localization clearly. Integro-differential operator (Daugman 1993) is adopted to search the satisfying circle matching the maximum variety of image intensity. Circle Hough Transform (Wildes 1997) searches for the circle parameters according to edge points that fall on perimeters of circles. The above two segmentation methods are extended to application scenarios with fewer constraints by introducing extra knowledge, such as total variance (Zhao and Ajay 2015), low-resolution contour (Sutra, Garcia-Salicetti, and Dorizzi 2012), pull and push model (He et al. 2008). Besides the circular assumption, the hypothesis of curve shapes is also accepted and applied in some works (Banerjee and Mery 2015; Shah and Ross 2009) to fit inner and outer boundaries.

Recently, the impressive progress of deep models in semantic segmentation promotes the development of deep iris segmentation. Deep iris segmentation does not rely on external knowledge but explores the intrinsic context in the images, which makes the boundary between iris segmentation and localization clearer. MFCNs (Liu et al. 2016) pioneers the application of FCN (Fully convolutional networks) to iris segmentation. In addition to FCN, encoder-decoder models (Arsalan et al. 2019) and U-Net models (Lozej et al. 2018; Lian et al. 2018) are also widely used in iris segmentation. CNNHT (Hofbauer, Jalilian, and Uhl 2019) introduces circular assumption and applies circular hough transforms to generate iris boundaries. IrisParseNet (Wang et al. 2020) develop the U-Net and proposes a multi-task attention network to learn iris mask, iris outer boundary, and pupil mask, simultaneously.

Visual transformer

In recent years, transformer makes impressive progress in multiple research fields, its rapid development attracts more and more attention from natural language processing (NLP) and computer vision (CV). Transformer models the long-range dependencies based on self-attention and builds a new architecture that is significantly different from the CNN and RNN. Vaswani et al. (Vaswani et al. 2017) first propose a transformer for a NLP task and defines its initial structure. With the proposition of transformer, many influential works emerge in multiple NLP tasks, such as BERT (Devlin et al. 2018), GPT2 (Radford et al. 2019), BigBird (Zaheer et al. 2020).

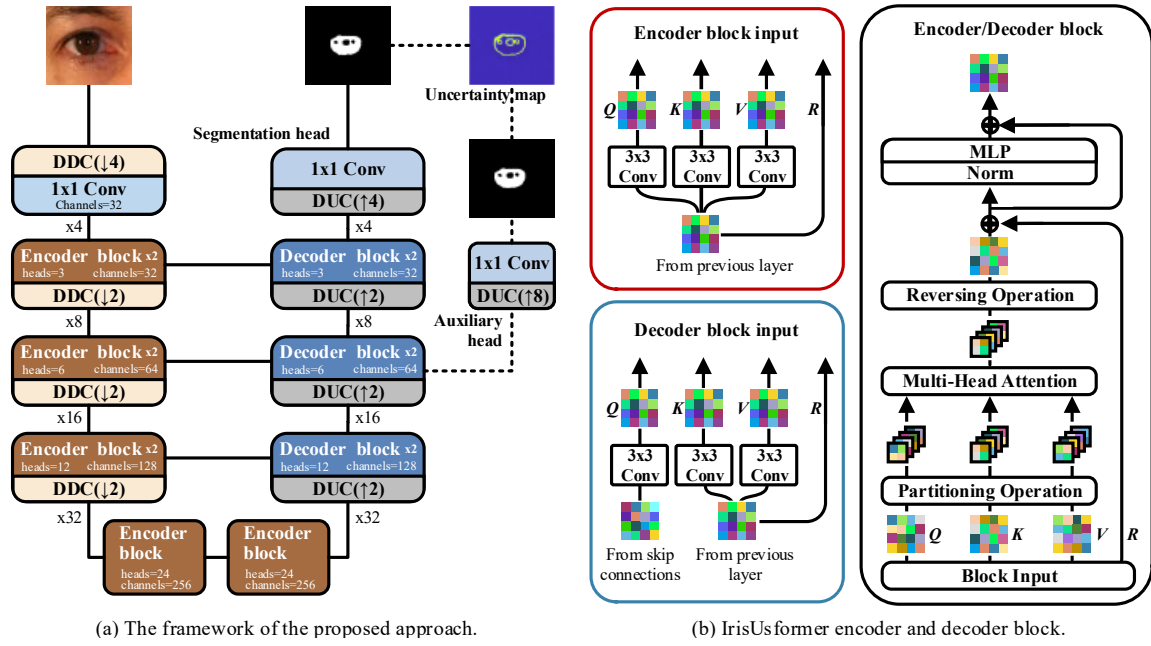


Figure 1: The framework of IrisUsformer. (a) The proposed IrisUsformer consists of an encoder, a bottleneck (two successive encoder blocks), a decoder, a segmentation head, and an auxiliary head. IrisUsformer estimates the uncertainty map according to segmentation predictions from the segmentation head and auxiliary head. (b) The detailed architectures of the encoder and decoder blocks in IrisUsformer. R is used here to illustrate the data flow.

The success of the transformer model in NLP quickly caught the eyes of the CV community. People start leveraging the transformer to explore the data context for the CV tasks. Initially, some approaches (Bello et al. 2019; Sun et al. 2019) develop existing CNN models by introducing partial modules of the transformer model, like self-attention. Their exciting experimental results encourage researchers to adopt a pure transformer model for the various CV tasks. In classification, ViT (Dosovitskiy et al. 2020) adopts patch embedding to generate sequential features for the image and builds a whole classification model using a pure transformer. For object detection, DETR (Carion et al. 2020) designs a new object detector based on transformers and discards the need for some hand-designed components like anchor boxes and Non-Maximum Suppression (NMS). For image generation, TransGAN (Jiang, Chang, and Wang 2021) leverages the power of the transformer and carefully designs a GAN model without convolutional operations. For semantic segmentation that is closely related to iris segmentation, there is a lot of works based on the transformer. SETR (Zheng et al. 2021) designs a pure transformer model for segmentation and models global context in every layer of the transformer. TransUnet (Chen et al. 2021) inserts a transformer module into U-Net to improve the feature generation of the bottleneck network. Swin transformer (Liu et al. 2021) proposes a shift window strategy to generate hierarchical feature maps.

Method

This section will introduce the technical details of the proposed IrisUsformer.

Architecture overview

The overall architecture of the proposed IrisUsformer is illustrated in Figure 1 (a). The proposed method adopts a U-shaped architecture consisting of encoder, bottleneck, decoder, skip connections, segmentation head, and auxiliary head. There are two basic units in our model, IrisUsformer encoder block for encoder and bottleneck, IrisUsformer decoder block for the decoder.

The encoder is alternately stacked by Dense Down-sampling Convolutions (DDCs) and encoder blocks. DDC is the down-sampling version of the Dense up-sampling Convolution (DUC), and it is used to reduce the input resolution for multi-scale feature generation. DDC divides the iris image into a grid of non-overlapping patches and arranges the pixels in the patch to different channels. Then, a 1×1 convolutional layer is placed at the end of DDC to project arranged features to arbitrary channels. More details about DDC are displayed in Appendix-A. DDC generates features with different spatial resolutions while encoder blocks model the local and global context of these features. In the forward propagation stage, an iris image travels through the combination of DDCs and encoder blocks to produce hierarchical feature representations.

As for the decoder, we design a symmetrical structure with the encoder. Specifically, IrisUsformer decoder blocks and DUCs construct the main body of the decoder. These DUCs are inserted into the decoder for an opposite goal of DDCs, i.e., increasing the spatial resolution of features. The decoder block leverages the cross-attention to guide the generation of segmentation prediction according to multi-scale

features from skip connections.

In the end, a $4 \times$ DUC and an 1×1 convolutional layer constitute the segmentation head. The segmentation head predicts a pixel-wise segmentation result via up-sampling. In addition, we adopt an auxiliary head for the uncertainty-wise weighting scheme. An auxiliary head is a free component for most semantic segmentation methods (Luo et al. 2019) since it does not appear in the inference stage. In the proposed approach, the auxiliary head is not only used for deep supervision (Lee et al. 2015) but also adopted for the uncertainty map estimation and uncertainty regularization. The auxiliary head has the same structure as the segmentation head, but it has an $8 \times$ up-sampling rather than $4 \times$ up-sampling.

In the subsequent parts, we would elaborate on each block.

Transformer block

Spatial position information is a vital clue in most CV tasks, and visual transformer generally applies positional embedding to provide pixels' positions. The recently proposed Swin transformer utilizes a window strategy to enhance the ability to spatial perception. Here, IrisUsformer further improves its spatial perception on the basis of the Swin transformer, as described below.

Encoder block In front of the self-attention module, the Swin transformer adopts linear projections to generate self-attention inputs, including Q (query matrices), K (key matrices), and V (value matrices). The linear projections aggregate the pixels in the same window but do not care about where the pixels are. One of the most extreme cases is the position of the corner of the window, each position is close to eight neighboring pixels. However, linear projection utilizes only three of them and other faraway pixels in the same window to generate attention inputs.

To further improve spatial perception, IrisUsformer uses a position-sensitive operation, convolutional projections, to replace linear projections to capture local spatial context for attention input generation, as shown in Figure 1 (b). Specifically, given feature maps $X \in \mathbb{R}^{C \times H \times W}$, the encoder block generates the attention inputs $Q = \phi_Q(X)$, $K = \phi_K(X)$, and $V = \phi_V(X)$, ϕ_Q , ϕ_K , and ϕ_V are the convolutional projections for attention inputs Q , K , V , respectively. Then, we utilize partitioning operation (PO) to divide the attention inputs into $\frac{H}{M} \times \frac{W}{M}$ non-overlapping patches of the same size $M \times M$ and tokenizes them. The self-attention with convolutional projections (CW-MSA) can be computed as follow:

$$\begin{aligned} \text{CW-MSA}(X) &= \text{Attention}(Q, K, V) \\ &= \text{RO}(A_1, \dots, A_N), \end{aligned} \quad (1)$$

where RO denotes the reverse operation to reverse the divided patches into a complete feature map with input resolution. $N = \frac{H}{M} \times \frac{W}{M}$ is the number of the non-overlapping patches. A_i is the attention output of the i -th patch, and it can be computed by

$$A_i = \text{SoftMax}\left(\frac{\text{PO}(Q)_i \text{PO}(K)_i^T}{\sqrt{d}} + B\right) \text{PO}(V)_i \quad (2)$$

where $\text{PO}(\cdot)_i$ denotes the i -th divided patch. B is the $M \times M$ relative position bias (Liu et al. 2021).

For two successive transformer blocks, IrisUsformer encoder block acts like Swin transformer blocks. The first one uses the regular partitioning strategy, and the second one uses the shifting strategy (named SCW-MSA). The continuous IrisUsformer encoder blocks can be formulated as:

$$\begin{aligned} \hat{X}^l &= \text{CW-MSA}(\text{LN}(X^{l-1})) + X^{l-1} \\ X^l &= \text{MLP}(\text{LN}(\hat{X}^l)) + \hat{X}^l \\ \hat{X}^{l+1} &= \text{SCW-MSA}(\text{LN}(X^l)) + X^l \\ X^{l+1} &= \text{MLP}(\text{LN}(\hat{X}^{l+1})) + \hat{X}^{l+1} \end{aligned} \quad (3)$$

where \hat{X}^l and X^l denote the outputs of the CW-MSA/SCW-MSA module and the Multi-Layer Perceptron (MLP) module of the l -th block. LN is the short for Layer Normalization.

In addition, in our implementation, IrisUsformer adjusts the pipeline of the transformer model by inserting tokenization and detokenization into the encoder block. This modification makes the encoder block easy to cooperate with convolutional modules, such as DUC and DDC in the proposed IrisUsformer.

Decoder block Considering that semantic segmentation is a pixel-wise task, it is vital to utilize hierarchical visual information in the decoder. To better leverage hierarchical visual features, we design the decoder version based on the encoder block.

Different from the encoder block, the decoder block employs cross-attentions to generate attention maps, as shown in Figure 1 (b). Specifically, the decoder block utilizes the hierarchical features from skip connections to generate Q . The change in attention inputs turns self-attention into cross-attention and allows multi-scale visual features to join the generation of the attention map. In the decoder, the cross attention fuses the low-level visual feature to modify the attention map and utilizes hierarchical knowledge for contextual aggregation.

The decoder block with two successive blocks also acts like the Swin transformer, i.e., the first one with partitioning strategy and the second one with shifting strategy.

Uncertainty-wise weighting scheme

As stated in Section I, the reliability of iris segmentation comes from the annotation and model uncertainty. To obtain a reliable segmentation, it is a critical and primary task to estimate the reliability of the segmentation prediction. Since the different depths correspond to the distinct subnetworks (Antorán, Allingham, and Hernández-Lobato 2020), there exists an apparent discrepancy between the segmentation results from the auxiliary head and the segmentation head. The discrepancy in segmentation results provides materials for the unreliability estimation (i.e., uncertainty estimation) (Saito et al. 2018a,b). Here, we learn an uncertainty map and propose a weighting scheme based on the estimated map.

Assuming that $P_s, P_a \in \mathbb{R}^{H \times W \times C}$ are the predictions from the segmentation head and auxiliary head, respectively.

H , W are the height and width of the segmentation predictions, C represents the number of the semantic classes. Then we can obtain the rough pixel-wise uncertainty map $M \in \mathbb{R}^{H \times W}$ according to the discrepancy of predictions. The computation process can be written as

$$M = - \sum_c (P_s \log P' + P_a \log P'), \quad (4)$$

where $P' = P_s + 0.5P_a$ denotes the average segmentation prediction. $c \in \{1, \dots, C\}$ represents the c -th semantic label, and $C = 2$ in iris segmentation.

With the uncertainty map, we propose an uncertainty-wise weighting scheme for segmentation loss by assigning high weight to the high-uncertainty region. Taking cross-entropy loss as an example, the weighted loss for the segmentation prediction P can be formulated as:

$$\mathcal{L}_{ce}(P) = - \sum_{h,w,c} MY \log P, \quad (5)$$

where Y denotes the ground-true segmentation mask.

To further reduce the negative impact of prediction uncertainty, we adopt an uncertainty regularization term for the proposed method. This regularization item reduces the uncertainty of segmentation predictions from a global perspective, and it can be formulated as:

$$\mathcal{R}_{kl} = \frac{\sum_{h,w} M}{HW} = \frac{- \sum_{h,w,c} (P_s \log P' + P_a \log P')}{HWC}. \quad (6)$$

In our implementation, we recommend ignoring the gradient from the segmentation loss to the uncertainty map for more stable convergence.

Objective function

In our model, there are two segmentation predictions from the segmentation head and auxiliary head, respectively. Both of them should be supervised by the ground truth segmentation mask. Besides, an uncertainty regularization term is adopted to reduce the model uncertainty.

Considering that iris segmentation is a pixel-wise binary classification problem, we adopt the uncertain-weighted version of the combination of cross-entropy loss and DiCE loss (Milletari, Navab, and Ahmadi 2016) for segmentation. The final objective function can be written as

$$\min \underbrace{\mathcal{L}_{ce}(P_s) + \mathcal{L}_{dice}(P_s)}_{\text{segmentation head}} + \underbrace{\mathcal{L}_{ce}(P_a) + \mathcal{L}_{dice}(P_a)}_{\text{auxiliary head}} + \alpha \mathcal{R}_{kl}, \quad (7)$$

where α is a trade-off parameter.

In Eq. 7, the formulation of weighted cross-entropy loss \mathcal{L}_{ce} is defined in Eq. 5, here, we provide the uncertainty weighting Dice loss

$$\mathcal{L}_{Dice}(P) = 1 - \frac{1}{C} \sum_c \frac{2 \sum_{h,w} M \times I + \epsilon}{\sum_{h,w} M \times U + \epsilon} \quad (8)$$

where K is the segmentation prediction. $I = PY$ and $U = K + Y$ represent the soft intersection and soft union between prediction and segmentation mask, respectively. ϵ is the smoothing factor.

Experiment

Databases

We evaluate the proposed IrisUsformer on three publicly available datasets. These three data sets cover various application scenarios involving variations in illumination (NIR and VIS), sensors, distance, etc.

CASIA-distance This dataset comes from CASIA-IrisV4, collected by the Chinese Academy of Sciences' Institute of Automation (CASIA). The images in CASIA-distance are captured at a long distance, and Wange et al. (Wang et al. 2020) selects ocular images from the first 40 subjects and labels their iris mask to build the segmentation dataset. The dataset consists of 400 images with a resolution of 640×480 , 300 images for training and 100 images for testing.

UBIRIS.v2 In the NICE-I competition, UBIRIS.v2 is employed to evaluate the performance of the iris system under visible illumination. Wang et al. (Wang et al. 2020) annotates the iris masks of these iris images and establishes the segmentation dataset of 500 images for training and 445 images for testing. The dataset adopts the image resolution of 400×300 pixels.

MICHE-I BipLab builds MICHE-I by capturing color iris images from mobile devices, including iPhone5, Samsung Galaxy S4, and Samsung Galaxy Tab2. All images in the dataset are acquired in uncontrolled conditions with visible illumination. Following the setting in IrisParseNet (Wang et al. 2020), the segmentation dataset has 680 images for training and 191 images for testing. Each image has a resolution of 400×400 .

Parameter setting and evaluation protocol

In subsequent experiments, we implement IrisUsformer on Pytorch, and set hyper-parameters as the following description. In the proposed method, there are two hyper-parameters for the proposed methods, a trade-off parameter in Eq. 7 and a smoothing factor in Eq. 8. We recommend $\alpha = 0.001$ and $\epsilon = 1$. As for optimizer, we employ mini-batch AdamW with a cyclical learning rate policy for 30000 iterations to train our model. Under the cyclic learning rate policy, the optimizer has a minimum learning rate of 10^{-5} and a maximum of 10^{-3} . The cycle length is set to 4000. We adopt the batch size of 10. To increase the data diversity, we borrow the data augmentation in IrisParseNet (Wang et al. 2020) but remove the random blur.

For iris semantic, previous competitions and works provide private quantitative indices for iris segmentation. We employ E1 (the average segmentation error rate) and F1 (the harmonic mean of precision and recall, it is equivalent to DICE for binary segmentation) to evaluate the proposed method. In addition, our experiment also adopts some general evaluation indices for semantic segmentation, such as mIoU and Acc.

Segmentation comparison

This section conducts segmentation experiments on three datasets to evaluate the proposed IrisUsformer. Here, we

Table 1: Quantitative comparison of iris segmentation methods (%). Note: 1) We highlight the best results in bold and underline the second-best results. 2) The state-of-the-art method and the baseline method are marked using † and §, respectively.

Methods	CASIA-distance				UBIRIS.v2				MICHE-1			
	E1↓	F1↑	mIoU↑	Acc↑	E1↓	F1↑	mIoU↑	Acc↑	E1↓	F1↑	mIoU↑	Acc↑
RTV-L	0.68	87.55	78.25	81.04	1.21	85.97	77.63	88.83	2.42	79.24	71.47	88.97
MFCNs	0.59	93.09	—	—	0.90	91.04	—	—	0.74	92.01	—	—
CNNHT	0.56	92.27	86.58	89.01	0.97	90.34	82.98	91.14	0.80	91.41	85.27	91.66
BiseNetv2	0.42	94.37	89.41	93.58	0.90	91.57	84.61	92.08	0.73	92.76	86.85	93.56
Unet	0.42	93.96	88.84	91.28	0.91	91.59	84.67	<u>92.50</u>	0.76	92.63	86.67	93.36
IrisParseNet †	0.41	94.25	89.52	93.29	0.84	<u>91.78</u>	<u>84.88</u>	92.31	0.66	<u>93.05</u>	<u>87.41</u>	<u>93.23</u>
Swin-base§	<u>0.40</u>	<u>94.52</u>	<u>89.68</u>	<u>93.91</u>	0.99	91.46	83.96	91.52	0.91	91.34	84.67	92.39
Ours	0.35	95.16	90.83	94.11	<u>0.85</u>	92.09	85.48	92.89	<u>0.68</u>	93.27	87.74	94.96

compare with seven representative iris segmentation approaches to demonstrate the effectiveness of IrisUsformer, including one non-deep learning model (RTV-L1 (Zhao and Ajay 2015)), five CNN models (MFCNs (Liu et al. 2016), CNNHT (Hofbauer, Jalilian, and Uhl 2019), BiseNetv2 (Yu et al. 2018, 2020), U-Net (Ronneberger, Fischer, and Brox 2015), IrisParseNet (Wang et al. 2020)) and one transformer model (Swin-base (Liu et al. 2021)). We preferentially records the experimental results in IrisParseNet (Wang et al. 2020) as the best performance of the compared methods and reports our reimplemented results as the supplement.

Table 1 lists summaries of the quantitative comparison. We highlight the best results in bold and underline the second-best results. Since we were unable to reproduce the satisfactory results of MFCNs, Table 1 does not show its results in terms of mIoU and Acc. Besides, Figure 2 visualizes the segmentation comparison maps. In the segmentation comparison map, we mark the true positive (correct prediction), false positive (wrong prediction in the non-iris region), and true negative pixels (wrong prediction in the iris region) using blue, red, and green, respectively.

In Table 1, the proposed IrisUsformer surpasses the compared methods in most indices (except E1) on multiple datasets. In terms of E1, IrisUsformer also shows competitive performance compared with the SOTA method (IrisParseNet). In addition, the red box indicates the segmentation details of different methods in Figure 2. According to these box, we can find that the proposed IrisUsformer makes a more accurate prediction for the pixels at the iris boundaries and pupil, which illustrates the performance advantage from a qualitative perspective. The superior performance demonstrates that long-range contextual aggregation is a discriminative clue for accurate iris segmentation. In particular, IrisUsformer is elaborately designed for better balance performance and computational consumption. Compared to IrisParseNet, IrisUsformer achieves better performance using 35% of Params and 19% FLOPs. The leading advantages in performance and computing resources indicate the efficacy of the proposed method in iris segmentation.

Compared with the baseline model (Swin-base), IrisUsformer shows a significant performance improvement on multiple indices. According to the average values of indices in Table 1, the proposed algorithm increase by 1.07%@F1,

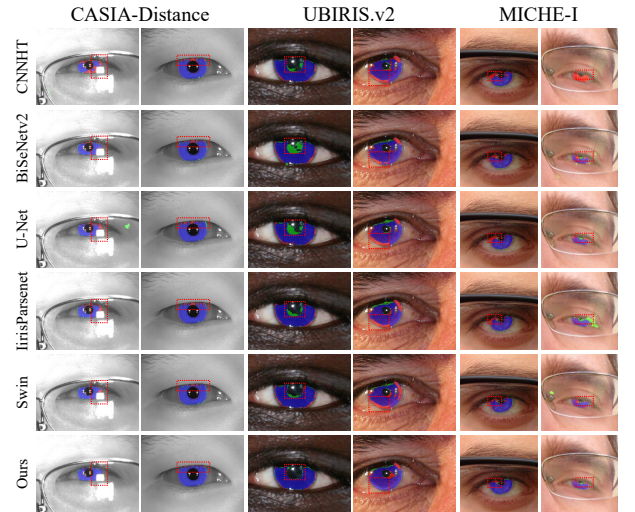


Figure 2: Qualitative segmentation comparison of different methods using segmentation comparison maps. Red boxes shows the segmentation details of different methods in each column. Appendix-C shows more qualitative comparison of different methods. (Best view in color and zoom in)

1.91%@mIoU, 1.38%@Acc. The performance improvement mainly comes from the following two aspects. First, IrisUsformer makes multiple efforts to capture more spatial information for accurate segmentation, such as convolutional projections and re-packaging transformer block. These efforts improve the model’s spatial perception, reducing segmentation bias. Second, the uncertainty-wise weighting scheme not only reduces the high-uncertainty region but also mitigates the overfitting in the reliable region with low uncertainty.

Visualization analysis

Regarding the proposed algorithm, there is still a problem in our minds. Does the uncertainty-wise weighting scheme really make the segmentation prediction more reliable? And how does it work? To investigate this problem, we provide a qualitative analysis by visualizing the uncertainty maps in Figure 3. Figure 3 plots the uncertainty maps and segmentation comparison maps of a testing image at the different

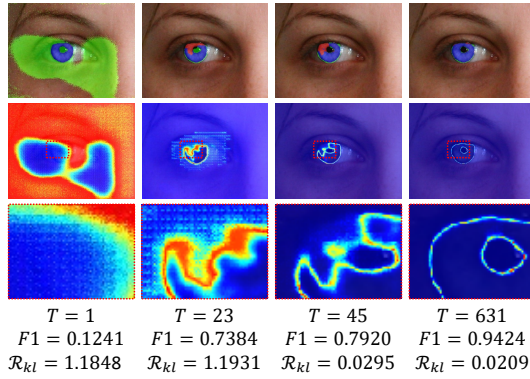


Figure 3: Segmentation comparison maps and uncertainty maps of a testing image at different training stages. Appendix-D provides more visualization results for segmentation comparison map and uncertainty maps at different training stages. (Best view in color and zoom in)

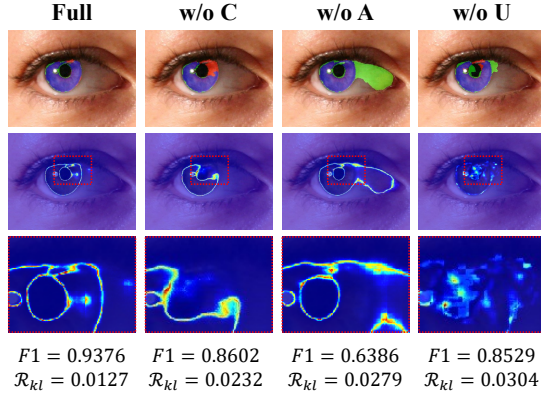


Figure 4: A representative visualization results for ablation study. The qualitative comparison illustrates the contribution of each module to segmentation accuracy.

training stages. The uncertainty map comes from Eq. 4. In Figure 3, the first row shows the segmentation comparison maps. The second row visualizes the uncertainty maps using the heat map. The third row provides a partial enlargement of the uncertainty maps. On the bottom row, we detail the information such as the number of epoch, F1, and uncertainty regularization.

In the early training stage, the randomly initialized model has poor segmentation accuracy. Obviously, the current model could not provide a reliable segmentation prediction, i.e., pixels of the uncertainty map have very high uncertainty. As iteration increases, the model gradually has better segmentation accuracy. The uncertainty map illustrates that high-uncertainty pixels are mainly located at the iris boundaries where the segmentation error occurs. In the subsequent optimization, high-uncertainty regions tend to produce higher loss values than other regions due to the weighting scheme. This weighted loss guide the model focuses on learning the segmentation knowledge in high-uncertainty regions. At the end of the iteration, segmentation errors rarely

Table 2: Quantitative comparison for the ablation study on these three datasets (%). Note: w/o C: discard convolutional projections and adopt linear projections. w/o A: replace cross-attention mechanism using concatenation and self-attention mechanism. w/o U: remove uncertainty-wise weighting scheme and uncertainty regularization. .

Methods		E1↓	F1/DICE↑	mIoU↑	Acc↑
Distance	Full	0.35	95.16	90.83	94.11
	w/o U	0.39	94.52	89.69	92.47
	w/o A	0.39	94.65	89.90	92.72
	w/o C	0.44	93.89	88.59	91.17
MICHE-IUBIRIS.v2	Full	0.85	92.09	85.48	92.89
	w/o U	0.92	91.54	84.56	92.93
	w/o A	0.91	91.56	84.61	92.93
	w/o C	0.92	91.23	84.05	91.14
MICHE-IUBIRIS.v2	Full	0.68	93.27	87.74	94.96
	w/o U	0.71	92.96	87.24	93.81
	w/o A	0.72	93.05	87.40	94.19
	w/o C	0.74	92.50	86.49	93.43

occur, but we can still find high-uncertainty regions in iris boundaries.

Ablation study

This section conduct the ablation study to understand the contribution of each module. The ablation study involves three ablation manners. w/o C: discard convolutional projections and adopt linear projections. w/o A: replace cross-attention mechanism using concatenation and self-attention mechanism. w/o U: remove uncertainty-wise weighting scheme and uncertainty regularization. Table 2 lists the quantitative results of the ablation study. Figure 4 visualizes the uncertainty maps and segmentation comparison maps of ablation models. Appendix-B provides relevant experimental analysis.

Conclusion

The paper proposes IrisUsformer for accurate and reliable iris segmentation to evade the impact of segmentation bias on recognition performance. Considering the iris segmentation is a pixel-wise task, we design a hierarchical encoder-decoder network and enhance its locality ability. On the one hand, the encoder of the proposed IrisUsformer utilizes the locality of convolutional projections to generate multi-scale features with more spatial information. On the other hand, we explore the guiding role of the cross-attention mechanism of our model in fusing multimodal features. In addition, to further improve the segmentation reliability, we estimate the prediction uncertainty and propose an uncertainty weighting scheme to make the model focus on the unreliable regions with high uncertainty. The experimental results on three iris segmentation datasets demonstrate the superior performance of IrisUsformer, while the ablation study and visualization results reflect the contributions of each module to performance improvement. Further exploration of this work should focus on iris segmentation driven by recognition accuracy.

References

- Antorán, J.; Allingham, J. U.; and Hernández-Lobato, J. M. 2020. Depth Uncertainty in Neural Networks. In *Advances in Neural Information Processing Systems 33: Annual Conference on Neural Information Processing Systems 2020, NeurIPS 2020, December 6-12, 2020, virtual*.
- Arsalan, M.; Kim, D. S.; Lee, M. B.; Owais, M.; and Park, K. R. 2019. FRED-Net: Fully residual encoder-decoder network for accurate iris segmentation. *Expert Systems with Applications*, 122: 217–241.
- Banerjee, S.; and Mery, D. 2015. Iris segmentation using geodesic active contours and grabcut. In *Image and Video Technology*, 48–60. Springer.
- Bazrafkan, S.; Thavalengal, S.; and Corcoran, P. 2018. An end to end deep neural network for iris segmentation in unconstrained scenarios. *Neural Networks*, 106: 79–95.
- Bello, I.; Zoph, B.; Vaswani, A.; Shlens, J.; and Le, Q. V. 2019. Attention augmented convolutional networks. In *Proceedings of the IEEE/CVF international conference on computer vision*, 3286–3295.
- Carion, N.; Massa, F.; Synnaeve, G.; Usunier, N.; Kirillov, A.; and Zagoruyko, S. 2020. End-to-end object detection with transformers. In *European Conference on Computer Vision*, 213–229. Springer.
- Chen, J.; Lu, Y.; Yu, Q.; Luo, X.; Adeli, E.; Wang, Y.; Lu, L.; Yuille, A. L.; and Zhou, Y. 2021. Transunet: Transformers make strong encoders for medical image segmentation. *arXiv preprint arXiv:2102.04306*.
- Daugman, J. G. 1993. High confidence visual recognition of persons by a test of statistical independence. *IEEE transactions on pattern analysis and machine intelligence*, 15(11): 1148–1161.
- Devlin, J.; Chang, M.-W.; Lee, K.; and Toutanova, K. 2018. Bert: Pre-training of deep bidirectional transformers for language understanding. *arXiv preprint arXiv:1810.04805*.
- Dosovitskiy, A.; Beyer, L.; Kolesnikov, A.; Weissenborn, D.; Zhai, X.; Unterthiner, T.; Dehghani, M.; Minderer, M.; Heigold, G.; Gelly, S.; et al. 2020. An image is worth 16x16 words: Transformers for image recognition at scale. *arXiv preprint arXiv:2010.11929*.
- He, Z.; Tan, T.; Sun, Z.; and Qiu, X. 2008. Toward accurate and fast iris segmentation for iris biometrics. *IEEE transactions on pattern analysis and machine intelligence*, 31(9): 1670–1684.
- Hofbauer, H.; Jalilian, E.; and Uhl, A. 2019. Exploiting superior CNN-based iris segmentation for better recognition accuracy. *Pattern Recognition Letters*, 120: 17–23.
- Jain, A. K.; Flynn, P.; and Ross, A. A. 2007. *Handbook of biometrics*. Springer Science & Business Media.
- Jiang, Y.; Chang, S.; and Wang, Z. 2021. Transgan: Two transformers can make one strong gan. *arXiv preprint arXiv:2102.07074*.
- Lee, C.-Y.; Xie, S.; Gallagher, P.; Zhang, Z.; and Tu, Z. 2015. Deeply-supervised nets. In *Artificial intelligence and statistics*, 562–570. PMLR.
- Lian, S.; Luo, Z.; Zhong, Z.; Lin, X.; Su, S.; and Li, S. 2018. Attention guided U-Net for accurate iris segmentation. *Journal of Visual Communication and Image Representation*, 56: 296–304.
- Liu, N.; Li, H.; Zhang, M.; Liu, J.; Sun, Z.; and Tan, T. 2016. Accurate iris segmentation in non-cooperative environments using fully convolutional networks. In *2016 International Conference on Biometrics (ICB)*, 1–8. IEEE.
- Liu, Z.; Lin, Y.; Cao, Y.; Hu, H.; Wei, Y.; Zhang, Z.; Lin, S.; and Guo, B. 2021. Swin Transformer: Hierarchical Vision Transformer using Shifted Windows. *arXiv preprint arXiv:2103.14030*.
- Lozej, J.; Meden, B.; Struc, V.; and Peer, P. 2018. End-to-end iris segmentation using u-net. In *2018 IEEE International Work Conference on Bioinspired Intelligence (IWOB)*, 1–6. IEEE.
- Luo, Y.; Liu, P.; Guan, T.; Yu, J.; and Yang, Y. 2019. Significance-aware information bottleneck for domain adaptive semantic segmentation. In *Proceedings of the IEEE/CVF International Conference on Computer Vision*, 6778–6787.
- Milletari, F.; Navab, N.; and Ahmadi, S.-A. 2016. V-net: Fully convolutional neural networks for volumetric medical image segmentation. In *2016 fourth international conference on 3D vision (3DV)*, 565–571. IEEE.
- Radford, A.; Wu, J.; Child, R.; Luan, D.; Amodei, D.; Sutskever, I.; et al. 2019. Language models are unsupervised multitask learners. *OpenAI blog*, 1(8): 9.
- Ronneberger, O.; Fischer, P.; and Brox, T. 2015. U-net: Convolutional networks for biomedical image segmentation. In *International Conference on Medical image computing and computer-assisted intervention*, 234–241. Springer.
- Saito, K.; Ushiku, Y.; Harada, T.; and Saenko, K. 2018a. Adversarial Dropout Regularization. In *International Conference on Learning Representations*.
- Saito, K.; Watanabe, K.; Ushiku, Y.; and Harada, T. 2018b. Maximum classifier discrepancy for unsupervised domain adaptation. In *Proceedings of the IEEE conference on computer vision and pattern recognition*, 3723–3732.
- Shah, S.; and Ross, A. 2009. Iris segmentation using geodesic active contours. *IEEE Transactions on Information Forensics and Security*, 4(4): 824–836.
- Sun, C.; Myers, A.; Vondrick, C.; Murphy, K.; and Schmid, C. 2019. Videobert: A joint model for video and language representation learning. In *Proceedings of the IEEE/CVF International Conference on Computer Vision*, 7464–7473.
- Sun, Z.; and Tan, T. 2008. Ordinal measures for iris recognition. *IEEE Transactions on pattern analysis and machine intelligence*, 31(12): 2211–2226.
- Sutra, G.; Garcia-Salicetti, S.; and Dorizzi, B. 2012. The Viterbi algorithm at different resolutions for enhanced iris segmentation. In *2012 5th IAPR International Conference on Biometrics (ICB)*, 310–316. IEEE.
- Vaswani, A.; Shazeer, N.; Parmar, N.; Uszkoreit, J.; Jones, L.; Gomez, A. N.; Kaiser, Ł.; and Polosukhin, I. 2017. Attention is all you need. In *Advances in neural information processing systems*, 5998–6008.

- Wang, C.; Muhammad, J.; Wang, Y.; He, Z.; and Sun, Z. 2020. Towards complete and accurate iris segmentation using deep multi-task attention network for non-cooperative iris recognition. *IEEE Transactions on information forensics and security*, 15: 2944–2959.
- Wildes, R. P. 1997. Iris recognition: an emerging biometric technology. *Proceedings of the IEEE*, 85(9): 1348–1363.
- Yu, C.; Gao, C.; Wang, J.; Yu, G.; Shen, C.; and Sang, N. 2020. Bisenet v2: Bilateral network with guided aggregation for real-time semantic segmentation. *arXiv preprint arXiv:2004.02147*.
- Yu, C.; Wang, J.; Peng, C.; Gao, C.; Yu, G.; and Sang, N. 2018. Bisenet: Bilateral segmentation network for real-time semantic segmentation. In *Proceedings of the European conference on computer vision (ECCV)*, 325–341.
- Zaheer, M.; Guruganesh, G.; Dubey, K. A.; Ainslie, J.; Alberti, C.; Ontanon, S.; Pham, P.; Ravula, A.; Wang, Q.; Yang, L.; et al. 2020. Big Bird: Transformers for Longer Sequences. In *NeurIPS*.
- Zhao, Z.; and Ajay, K. 2015. An accurate iris segmentation framework under relaxed imaging constraints using total variation model. In *Proceedings of the IEEE international conference on computer vision*, 3828–3836.
- Zhao, Z.; and Kumar, A. 2017. Towards more accurate iris recognition using deeply learned spatially corresponding features. In *Proceedings of the IEEE international conference on computer vision*, 3809–3818.
- Zheng, S.; Lu, J.; Zhao, H.; Zhu, X.; Luo, Z.; Wang, Y.; Fu, Y.; Feng, J.; Xiang, T.; Torr, P. H.; et al. 2020. Rethinking Semantic Segmentation from a Sequence-to-Sequence Perspective with Transformers. *arXiv preprint arXiv:2012.15840*.
- Zheng, S.; Lu, J.; Zhao, H.; Zhu, X.; Luo, Z.; Wang, Y.; Fu, Y.; Feng, J.; Xiang, T.; Torr, P. H.; et al. 2021. Rethinking semantic segmentation from a sequence-to-sequence perspective with transformers. In *Proceedings of the IEEE/CVF Conference on Computer Vision and Pattern Recognition*, 6881–6890.
- Zheng, Z.; and Yang, Y. 2021. Rectifying pseudo label learning via uncertainty estimation for domain adaptive semantic segmentation. *International Journal of Computer Vision*, 129(4): 1106–1120.

Supplementary Material for “Toward Accurate and Reliable Iris Segmentation Using Uncertainty Learning”

Jianze Wei^{1,2}, Huaibo Huang², Muyi Sun², Ran He², Zhenan Sun²

¹ School of Artificial Intelligence, University of Chinese Academy of Sciences, Beijing, China

² CRIPAC & NLPR, Institute of Automation, Chinese Academy of Sciences, Beijing, China
{jianze.wei, huaibo.huang, muyi.sun}@cripac.ia.ac.cn, {rhe, znsun}@nlpr.ia.ac.cn

Appendix

This supplementary includes:

- The network architectures of DUC and DDC.
- Detailed analysis for the ablation study.
- More visualization results for segmentation comparison.
- More visualization results to demonstrate how the uncertainty-wise weighting scheme works.

A. Network architecture of DUC and DDC

Dense Up-sampling Convolution (DUC) and Dense Down-sampling Convolution (DDC) are two important CNN-tyle modules in the proposed IrisUsformer. They are applied in our model to change the resolution of the feature map. To facilitate the reproduction of our works, we detail these two modules in this section.

DUC is proposed for pixel-level semantic segmentation (Wang et al. 2018), and IrisUsformer utilizes it to increase the resolution of the input feature map in the decoder. DUC consists of a convolutional layer, batch normalization layer, an activation function, and a pixel shuffle layer, as shown in Figure 1 (a).

DDC is designed as an extension of DUC. In IrisUsformer, we apply it in the encoder to reduce the resolution of the input feature map. DDC has almost the same components as DUC but replaces a pixel shuffle layer with a pixel-unshuffle layer (Shi et al. 2016; Zhao et al. 2020). The network architecture of DDC is visualized in Figure 1 (b).

B. Detailed analysis for ablation study

In this section, we make the ablation study to understand the contribution of each module to performance improvement. The ablation study involves three ablation manners described as following. w/o C: discard convolutional projections prior to the self-attention module and adopt linear projections. w/o A: replace cross-attention mechanism using concatenation and self-attention mechanism. w/o U: remove uncertainty-wise weighting scheme and uncertainty regularization. Table 1 lists the quantitative results of the ablation study.

Copyright © 2022, Association for the Advancement of Artificial Intelligence (www.aaai.org). All rights reserved.

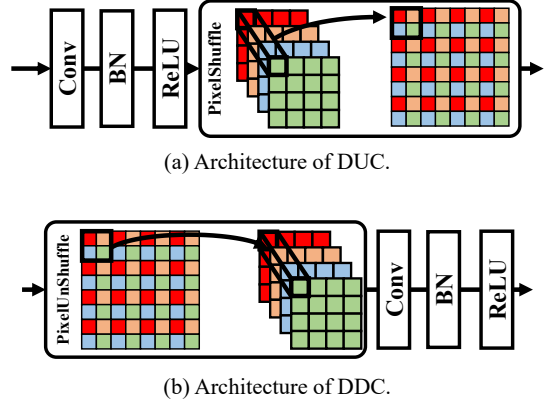


Figure 1: Visualization results. The true positive, false positive, and true negative pixels are marked with blue, red, and green, respectively.

In Table 1, The value changes of the evaluation indices reflect the effectiveness of different modules on segmentation performance.

1. Degradation in "w/o U" manner. As the degraded model of the proposed method, IrisUsformer in "w/o U" manner has a poorer segmentation performance on these three datasets. The performance decline illustrates the contributions of the uncertainty-wise weighting scheme and uncertainty regularizer on segmentation. In addition, compared with experimental results on MICHE-1, the ablation model shows a significant performance degradation ($\downarrow 0.64\%$ and $\downarrow 0.55\%$ @F1) on CASIA-distance and UBIRIS.v2 when we remove the modules relevant to uncertainty. We believe that the acquisition settings for CASIA-distance and UBIRIS.v2 cause serious degradation. Images in CASIA-distance are captured at a long-range distance, while images in UBIRIS.v2 are captured under the "on-the-move and at-a-distance" (Wang et al. 2020) setting. These settings mean that these images are exponentially affected by uncertain acquisition factors. Therefore, the uncertainty-wise weighting scheme and uncertainty regularizer have more significant performance improvement on CASIA.v4-distance.

2. Degradation in "w/o A" manner. The complete IrisUsformer shows superior performance than the ablation model

Table 1: Quantitative comparison for the ablation study on these three datasets (%). Note: w/o C: discard convolutional projections and adopt linear projections. w/o A: replace cross-attention mechanism using concatenation and self-attention mechanism. w/o U: remove uncertainty-wise weighting scheme and uncertainty regularization. .

Methods		E1↓	F1/DICE↑	mIoU↑	Acc↑
Distance	Full	0.35	95.16	90.83	94.11
	w/o U	0.39	94.52	89.69	92.47
	w/o A	0.39	94.65	89.90	92.72
	w/o C	0.44	93.89	88.59	91.17
MICHE-IUBIRIS.v2	Full	0.85	92.09	85.48	92.89
	w/o U	0.92	91.54	84.56	92.93
	w/o A	0.91	91.56	84.61	92.93
	w/o C	0.92	91.23	84.05	91.14
MICHE-IUBIRIS.v2	Full	0.68	93.27	87.74	94.96
	w/o U	0.71	92.96	87.24	93.81
	w/o A	0.72	93.05	87.40	94.19
	w/o C	0.74	92.50	86.49	93.43

in "w/o A" manner. The performance advantage is contributed by the cross-attention. It actively fuses the hierarchical feature into segmentation prediction via modification of the attention map, leading to accurate segmentation. In addition, compared with the uncertainty weighting scheme, cross-attention in decoder provide similar performance improvement on various datasets.

3. *Degradation in "w/o C" manner:* Compared with other manners, "w/o C" causes more obvious changes in multiple indices, which means that convolutional projections heavily affect the segmentation performance of IrisUsformer. Specifically, IrisUsformer in "w/o C" drops by more than 0.77% in F1 on all datasets. Different from linear projection, convolutional projection is more sensitive to spatial position. It helps attention modules to focus on neighboring pixels rather than the pixels in the same patch. In other words, convolutional projection raises the ability of IrisUsformer to capture local spatial information. The performance degradation in "w/o C" manner supports our viewpoint.

C. Segmentation comparison

This section provides more qualitative comparison of different methods in Figure 2. In Figure 2, we visualize segmentation comparison maps and mark the true positive (correct prediction), false positive (wrong prediction in the non-iris region), and true negative pixels (wrong prediction in the iris region) using blue, red, and green, respectively.

According to Figure 2, these visualization results support the previous analysis that the proposed IrisUsformer shows more accurate segmentation for the pixels at the iris boundaries and pupill. The performance advantage indicates that the proposed method has more accurate and reliable prediction for iris segmentation.

D. Visualization analysis

To better understand how uncertainty-wise weighting scheme works, the section plots more visualization results for uncertainty maps of a testing image at different training stage in Figure 3. These visualization results support the previous analysis.

References

- Shi, W.; Caballero, J.; Huszár, F.; Totz, J.; Aitken, A. P.; Bishop, R.; Rueckert, D.; and Wang, Z. 2016. Real-time single image and video super-resolution using an efficient sub-pixel convolutional neural network. In *Proceedings of the IEEE conference on computer vision and pattern recognition*, 1874–1883.
- Wang, C.; Muhammad, J.; Wang, Y.; He, Z.; and Sun, Z. 2020. Towards complete and accurate iris segmentation using deep multi-task attention network for non-cooperative iris recognition. *IEEE Transactions on information forensics and security*, 15: 2944–2959.
- Wang, P.; Chen, P.; Yuan, Y.; Liu, D.; Huang, Z.; Hou, X.; and Cottrell, G. 2018. Understanding convolution for semantic segmentation. In *2018 IEEE winter conference on applications of computer vision (WACV)*, 1451–1460. IEEE.
- Zhao, Y.; Po, L.-M.; Yan, Q.; Liu, W.; and Lin, T. 2020. Hierarchical regression network for spectral reconstruction from RGB images. In *Proceedings of the IEEE/CVF Conference on Computer Vision and Pattern Recognition Workshops*, 422–423.

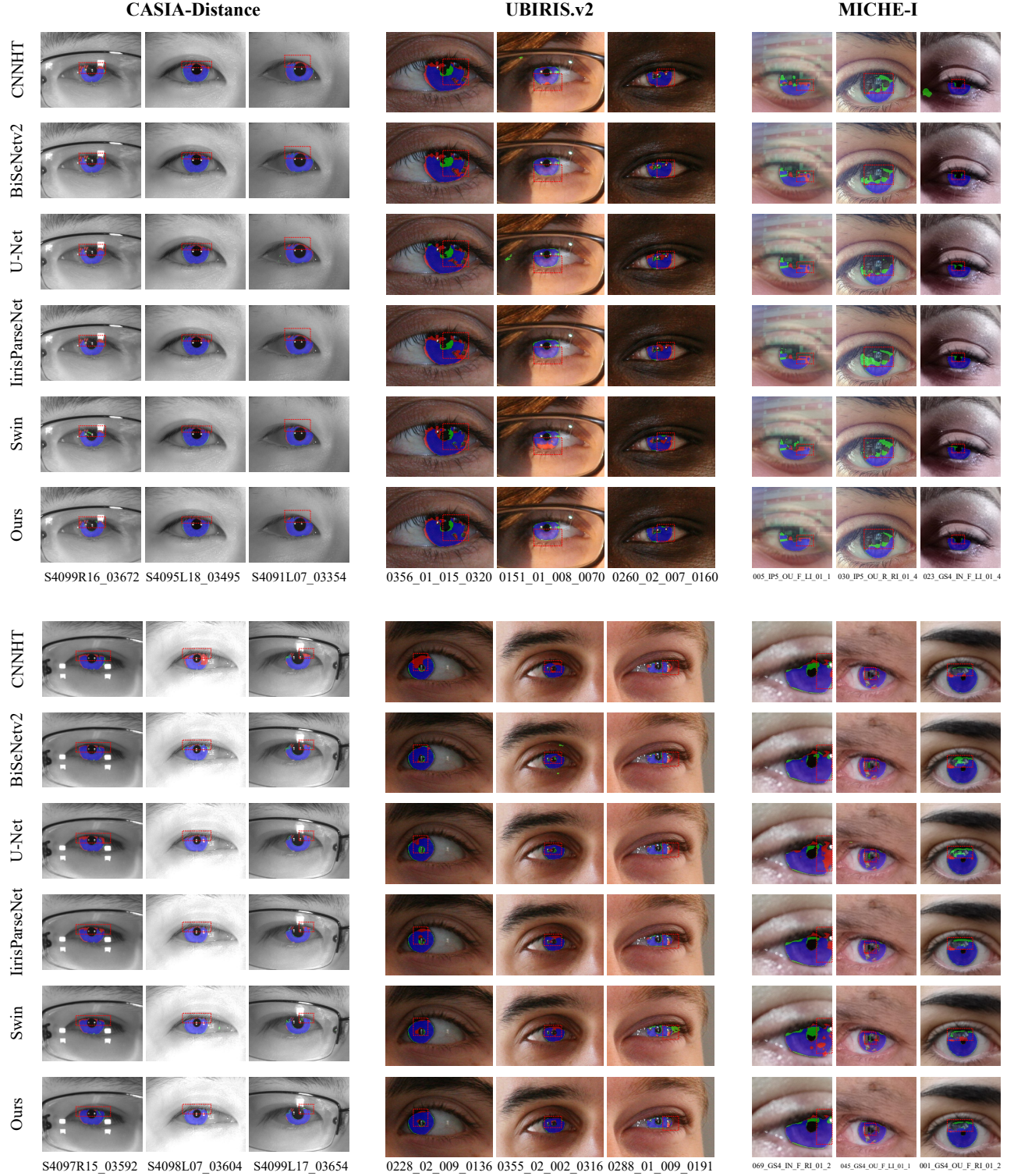


Figure 2: Qualitative segmentation comparison of different methods using segmentation comparison maps. The true positive (correct prediction), false positive (wrong prediction in the non-iris region), and true negative pixels (wrong prediction in the iris region) are marked using blue, red, and green, respectively. Red boxes shows the segmentation details of different methods in each column. (Best view in color and zoom in)

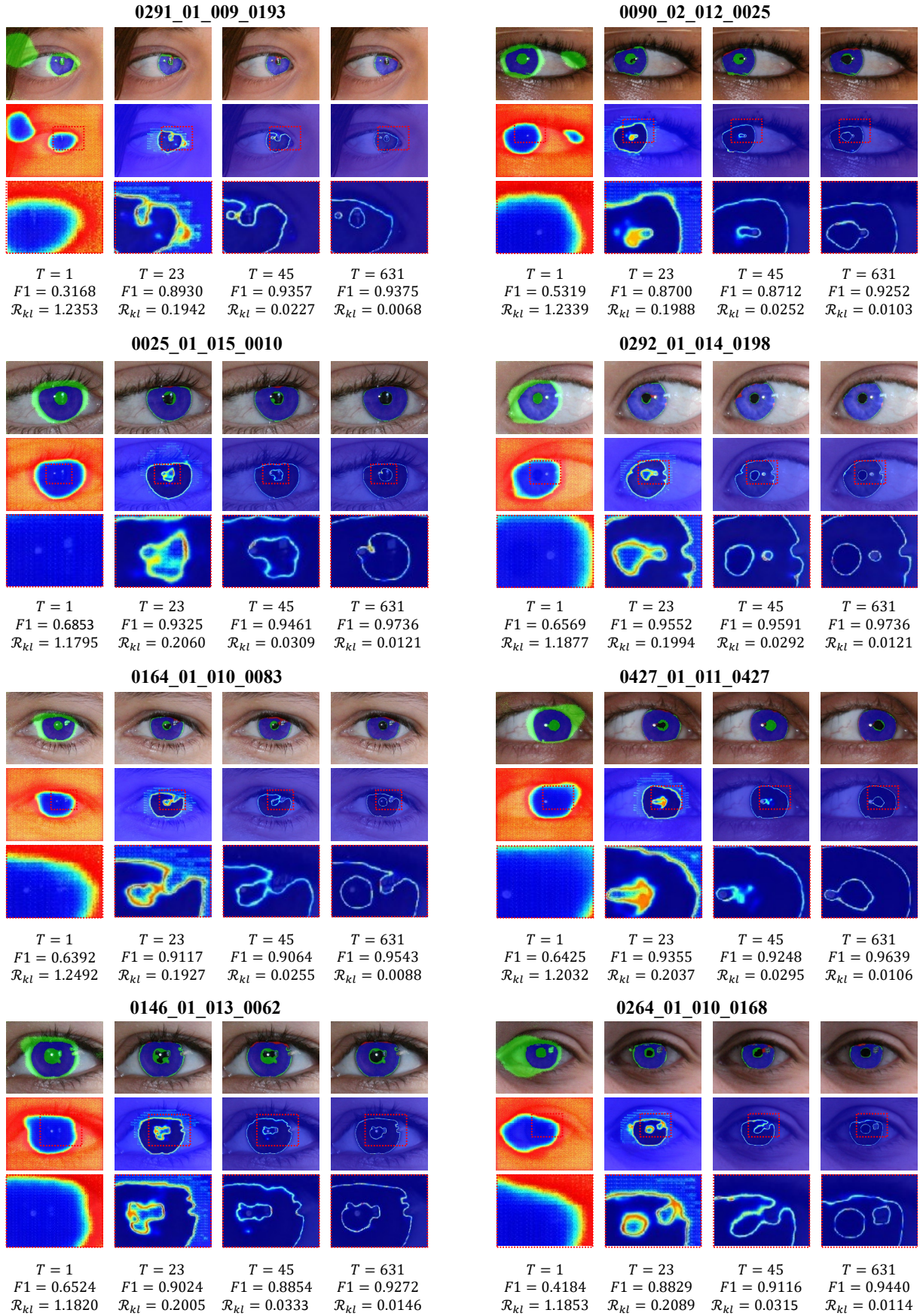


Figure 3: Segmentation comparison maps and uncertainty maps of testing images at different training stages. The first row shows the segmentation comparison maps. The second row visualizes the uncertainty maps using the heat map. The third row provides a partial enlargement of the uncertainty maps. On the bottom row, we detail the information such as the number of epoch, F1, and uncertainty regularization. (Best view in color and zoom in)